

## Optical-microwave double-resonance spectroscopy of highly excited Rydberg states of ytterbium

H. Maeda, Y. Matsuo, and M. Takami

*RIKEN, The Institute of Physical and Chemical Research, Wako, Saitama 351-01, Japan*

A. Suzuki

*Faculty of Engineering, University of Tokyo, 7-3-1 Hongo, Bunkyo-ku, Tokyo 113, Japan*

(Received 5 June 1991)

Microwave transitions between the neighboring levels that belong to the  $^1S_0$ ,  $^1P_1$ , and  $^1D_2$  Rydberg series of ytterbium are studied for the principal quantum number ranging from 33 to 57. The term values and the quantum defects are determined by means of the general Rydberg-Ritz formula. The determined quantum defects show large linear energy dependence. The Zeeman effect measured for three  $^1P_1$  and one  $^1D_2$  Rydberg states under a weak external magnetic field is discussed.

PACS number(s): 32.60.+i, 32.30.Bv, 32.80.Rm

### I. INTRODUCTION

Optical-microwave double-resonance spectroscopy is one of the most powerful techniques of studying the structure of highly excited Rydberg states of atoms and molecules. Since the linewidth is usually limited by the interaction time of microwave radiation with Rydberg atoms and molecules, spectral resolution of higher than 100 kHz is easily obtained owing to the long lifetime of Rydberg states. A number of such experiments have been reported in the past one and a half decades, including the study of quantum defects and fine-structure intervals [1–13], hyperfine structures [7], isotope shifts [11], core polarizabilities [4, 12, 13] Rabi oscillation process [14], weak configuration interactions between Rydberg series and a valence state in the electric field [15], etc. However, all of these studies have been limited to the Rydberg states of He, alkali-metal atoms (Li, Na, Cs) and alkaline-earth atoms (Ca, Ba). In this paper, we report the first optical-microwave double-resonance spectroscopy on highly excited Rydberg states of ytterbium.

The configuration of the ground state of ytterbium is  $4f^{14}6s^2$ , and hence the main part of its spectrum behaves like the alkaline-earth atoms. However, as is well known, the closed  $4f$  subshell of ytterbium is easily broken and, as a consequence, the  $4f^{14}6snl$  Rydberg series, which converge to the first ionization limit, are perturbed not only by the  $4f^{14}nln'l'$ -type valence levels, but also by the  $4f^{13}nln'l'n''l''$ -type valence levels in a various way over the extended energy range.

The Rydberg states of ytterbium have been studied by Wyart and Camus [16], Camus, Débarre, and Morillon [17], Aymer *et al.* [18, 19], and several other groups [20–23]. However, due to its spectral complexity the energy-level structure in the vicinity of the first ionization limit is still not well understood and, accordingly, more extensive and accurate measurements of Rydberg states are desirable. Although there is a number of spectroscopic studies on ytterbium, the experiment with high spectral resolution is still a rare case to our knowledge [21–23].

The purpose of this paper is to present the precise transition frequencies between levels belonging to the  $4f^{14}6sns^1S_0$ ,  $4f^{14}6snp^1P_1$ , and  $4f^{14}6snd^1D_2$  Rydberg series of ytterbium with an accuracy of better than 1 MHz, and to discuss the  $n$  dependence of the quantum defects of each series. In order to study the configuration and the spin-orbit interaction in the  $^1P_1$  and  $^1D_2$  series, the Landé  $g$  factors have been measured for some of these levels in a weak external magnetic field. In Sec. II our experimental setup and procedure are described. In Sec. III the experimental data is presented followed by an analysis based on the general Rydberg-Ritz formula. The Zeeman effect on some of the Rydberg levels under weak magnetic field is reported as well.

### II. EXPERIMENT

The principal part of our experimental setup and the techniques are similar to those described in Ref. [3]. A schematic diagram of the setup is illustrated in Fig. 1(a). Highly excited Rydberg states of ytterbium were prepared by an irradiation of two pulsed dye-laser beams onto the atomic beam generated by a resistively heated oven. The first dye-laser beam at 398.8 nm excited the ytterbium atoms from the ground state  $4f^{14}6s^2^1S_0$  to the intermediate state  $4f^{14}6s6p^1P_1$ . The second laser excited the atoms further up to one of the even  $4f^{14}6sns^1S_0$  or  $4f^{14}6snd^1D_2$  Rydberg states as shown in Fig. 2.

The transition between the Rydberg states were induced by continuous microwave radiation from several millimeter-wave klystrons, which covered the frequency range of 18–56 GHz and 62–78 GHz with a typical output power of a few hundred mW. Several attenuators of up to  $\sim 70$  dB were used to reduce the microwave power in order to avoid saturation broadening and ac Stark shift of the spectral line. The transition frequencies were calibrated with a frequency marker produced by mixing the microwave and the harmonics of a X-band Gunn oscillation.

tor, the frequency of which was measured directly with a microwave frequency counter.

The detection of microwave transition was based on the selective field ionization technique [24]. About  $5 \mu\text{sec}$  after the laser excitation, pulsed electric field of appropriate intensity (max  $\sim 600 \text{ V/cm}$ ) with  $3\text{-}\mu\text{s}$  time duration was applied between a pair of metal electrodes in order to ionize the atoms in the upper state of the microwave transition selectively and to accelerate the produced ions toward a secondary-electron multiplier through a grid prepared in the middle of the upper electrode [see Fig. 1(b)].

Then the ion signals were amplified and averaged with a boxcar integrator.

### III. RESULTS AND DISCUSSION

#### A. Observation of microwave transitions

Figure 3 shows the energy-level diagram of ytterbium relevant to the present experiment. The high Rydberg states studied in the present work are in the region of the  $LS\text{-}jj$  transition and therefore definite designation of the

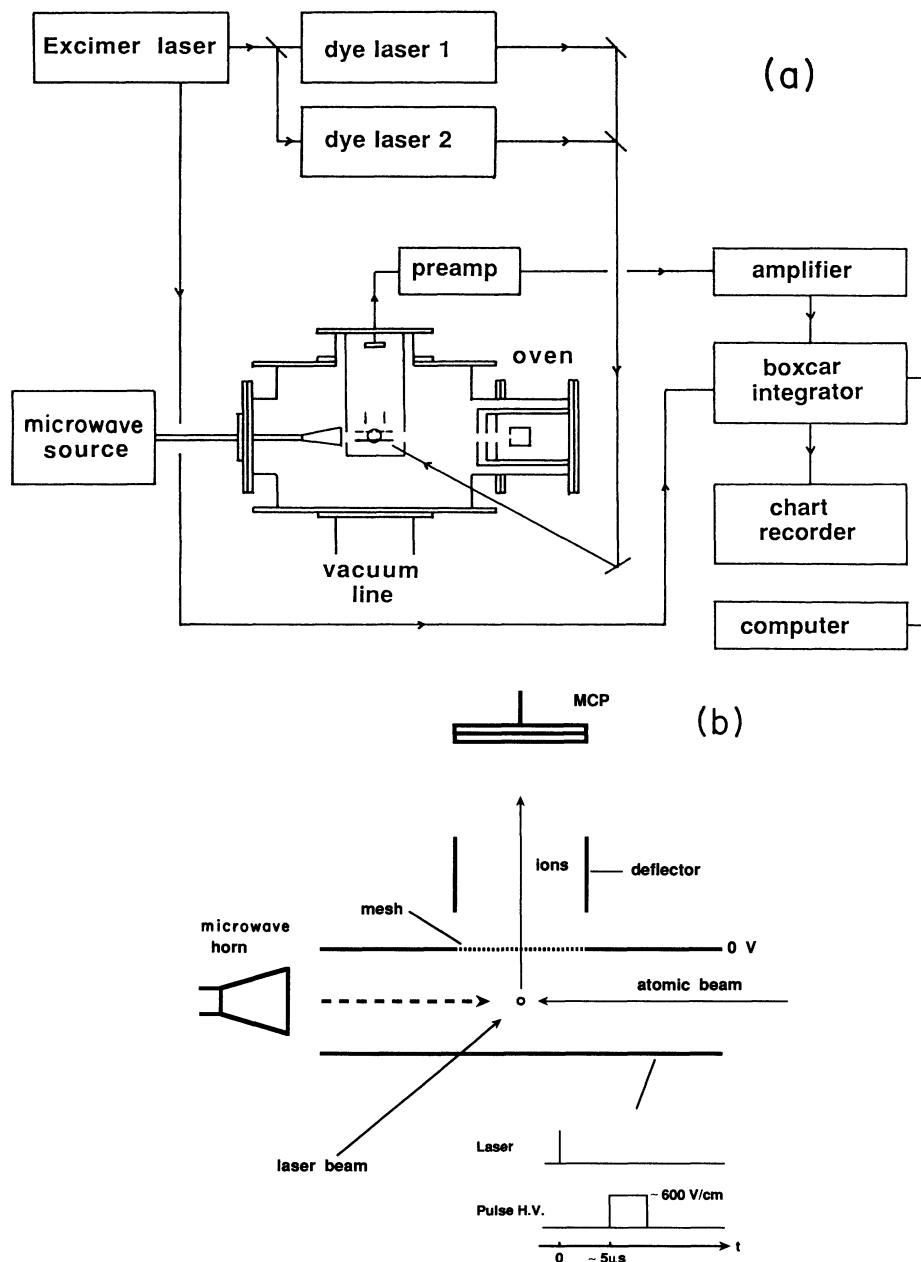


FIG. 1. (a) A schematic diagram of the experimental setup. (b) A sketch of the interaction region of atoms, pulsed laser, and microwave with a diagram showing the time sequence of pulsed laser and pulsed electric field.

states by  $LS$  coupling is sometimes difficult. In fact the two optically measured  $P_1$  series have been designated by  $P_{\pm}$  for the upper (+) and lower (-) levels for a given  $n$  state [19]. However, we will use the customary notation,  $^1P_1$  and  $^3P_1$ , for  $P_+$  and  $P_-$  throughout the work since the singlet-triplet mixing is not prominent in the studied energy region. The present optical excitation through the  $4f^{14}6s6p^1P_1$  intermediate state prepares the  $^1S_0$ ,  $^1D_2$ , and  $^3D_2$  series reported in Ref. [17]. However, the  $^3D_2$  series were weak, and could not be identified for  $n \geq 29$  since the series overlapped with the much stronger  $^1D_2$  series.

The measured microwave transitions are one-photon transitions for

$$6snp^1P_1 \leftarrow 6sns^1S_0 \quad (n = 35, 36, 39 \sim 53),$$

$$6s(n+1)p^1P_1 \leftarrow 6sns^1S_0 \quad (n = 52 \sim 55),$$

$$6s(n+2)p^1P_1 \leftarrow 6snd^1D_2 \quad (n = 43 \sim 45, 47 \sim 53),$$

two-photon transitions for

$$6s(n+1)s^1S_0 \leftarrow 6sns^1S_0 \quad (n = 39 \sim 41, 43 \sim 56),$$

$$6s(n+1)d^1D_2 \leftarrow 6snd^1D_2 \quad (n = 38, 39, 41 \sim 55),$$

$$6s(n-1)d^1D_2 \leftarrow 6sns^1S_0 \quad (n = 34, 36 \sim 49),$$

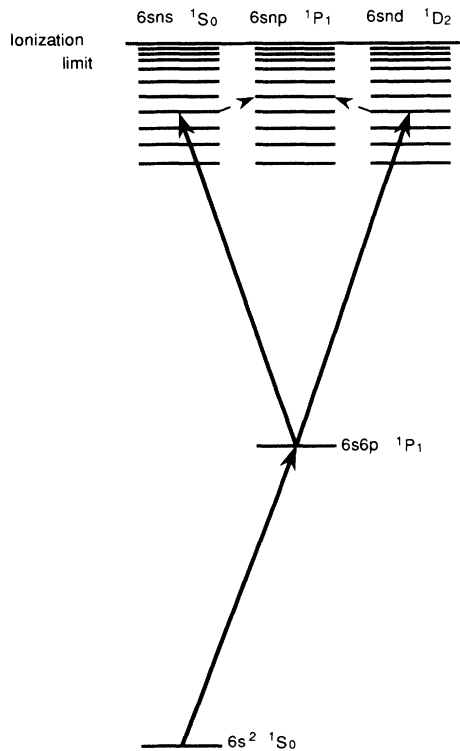


FIG. 2. Excitation scheme of ytterbium atom to the highly excited Rydberg states. The solid arrows indicate the two-step optical excitation via the  $6s6p^1P_1$  intermediate state, and broken arrows indicate the microwave transitions.

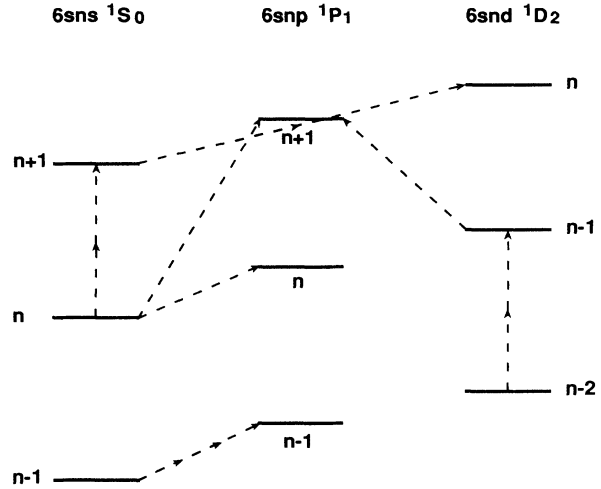


FIG. 3. Energy-level diagram of Rydberg ytterbium showing the types of transitions observed in the present work. Arrows indicate the microwave transitions.

and three-photon transitions for

$$6snp^1P_1 \leftarrow 6sns^1S_0 \quad (n = 34 \sim 36),$$

respectively.

The above assignments are based primarily on the difference of optical-transition frequencies reported in Refs. [18] and [19]. The assignments were confirmed by the Zeeman splitting observed under a weak magnetic field as described in the final section. This method was particularly helpful for the assignment of  $6snp^1P_1 \leftarrow 6sns^1S_0$  three-photon transitions which were found during the extensive search for the  $6snp^3P_1 \leftarrow 6sns^1S_0$  transitions. Because the apparent  $g$  factors of these transitions were approximately 1/3 of those measured in the one-photon transitions, we concluded that they were the three-photon microwave transitions to the  $^1P_1$  states. The failure to observe the  $6snp^3P_1 \leftarrow 6sns^1S_0$  one-photon transitions and  $6snd^3D_2 \leftarrow 6sns^1S_0$  two-photon transitions will be simply due to small singlet character of the  $^3P_1$  and  $^3D_2$  states in the studied region [18, 23].

A part of the observed transitions form the following closed loops:

$$\begin{array}{ccc} 6snd^1D_2 & \leftarrow & 6s(n+1)s^1S_0 \\ \uparrow & & \uparrow \\ 6s(n-1)d^1D_2 & \leftarrow & 6sns^1S_0, \end{array}$$

which are used to find the accuracy of frequency measurement. Among eight loops, six showed the residual frequency less than 1 MHz indicating high reliability of the measured frequencies.

Figure 4 shows a typical example of the observed spectral lines. The linewidth of the microwave transitions

in the present work is limited by saturation broadening, finite interaction time, frequency jitter of the klystron, geomagnetic field, and stray electric field. In some of the one-photon transitions, we failed to reduce the saturation broadening below a few MHz [fullwidth of half maximum (FWHM)] due to the huge transition dipole moments and the leakage of microwave field through the unknown route. This origin of the large linewidth was confirmed by the experimental fact that the linewidth of  $6s35p^1P_1 \leftarrow 6s35s^1S_0$  transition was 4.0 MHz for the one-photon transition while it was 1.2 MHz for the three-photon transition (three times the apparent width) which requires higher microwave power to saturate. For the other transitions, the observed linewidths were in the range of 500 kHz to 1 MHz. In Fig. 5 a typical trace of the  $6s36p^1P_1 \leftarrow 6s36s^1S_0$  transition under a weak magnetic field is shown. The linewidth of 240 kHz roughly corresponds to the width due to 5- $\mu$ sec interaction time. All the measured frequencies are given in Tables I-V with the linewidths (FWHM) as a measure of experimental uncertainties.

The nuclear hyperfine structure by the odd ytterbium nuclei ( $^{171}\text{Yb}:I = 1/2$ ,  $^{173}\text{Yb}:I = 5/2$ ) has been studied in the optical transitions to the  $^1,^3P_1$  and  $^3D_2$  high Rydberg states [21, 22]. The hyperfine splitting is mostly due to the  $6s$  electron of the ion core, and extends over several GHz. In the microwave transition the hyperfine splitting of a similar size is expected while the isotope

shift, which was clearly resolved in the optical spectrum, should be negligibly small. As a consequence, the intensity of the strongest hyperfine satellite is less than 10% of the main peak. Although the hyperfine satellite lines were carefully searched for, we are not yet successful in the observation probably due to the lack of sensitivity.

### B. Analysis of the frequency data

It is well established to express the transition frequencies between Rydberg states by the following general Rydberg-Ritz formula with  $L$ ,  $S$ , and  $J$  notation,

$$E_{LSJ}(n) = I - \frac{R}{[n - \delta_{LSJ}(n)]^2}, \quad (1)$$

where  $E_{LSJ}(n)$  is the energy of the Rydberg state,  $I$  is the convergence limit of the Rydberg series,  $R$  is the Rydberg constant for the corresponding atom, and

$$\delta_{LSJ}(n) = \delta_{LSJ0} + \frac{\delta_{LSJ1}}{[n - \delta_{LSJ}(n)]^2} + \dots \quad (2)$$

is the quantum defect which is expanded in a power series of the inverse square of the effective quantum number  $n^* \equiv n - \delta_{LSJ}(n)$  to include the energy dependence of quantum defect [25].

When a series is perturbed by valence levels, and such is the usual case for a complex electron system, the influ-

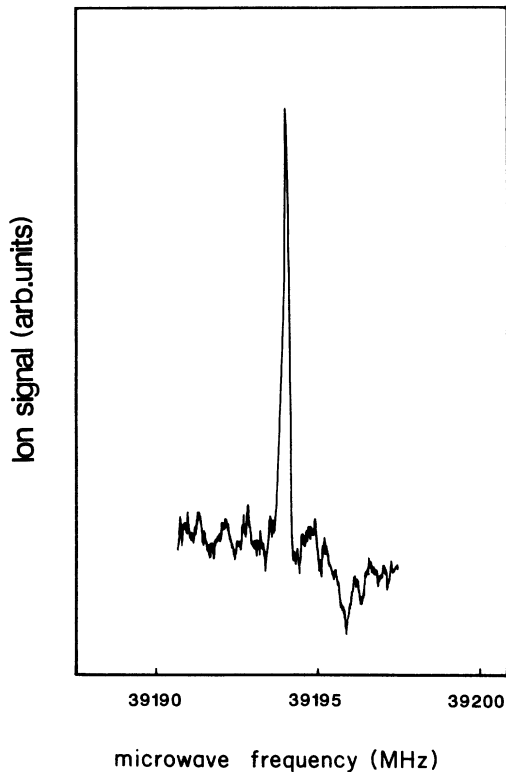


FIG. 4. A recording of the  $6s47d^1D_2 \leftarrow 6s46d^1D_2$  two-photon microwave transition.

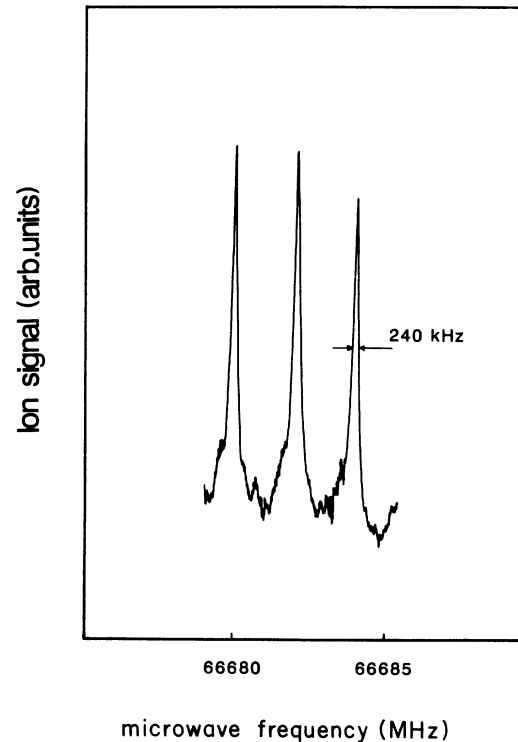


FIG. 5. A Zeeman pattern of the  $6s36p^1P_1 \leftarrow 6s36s^1S_0$  transition under a 4.1-G external magnetic field.

ence of local perturbations should be included by adding the following terms to Eq. (2),

$$\sum_i \frac{\text{const}(i)}{E_{LSJ}(n) - E_{P(i)}} \quad (3)$$

where  $E_{P(i)}$  is the energy of the  $i$ th perturber. This modified Rydberg-Ritz formula is usually called the Langer's formula [26–28].

A number of optical studies on ytterbium have revealed the occurrence of several perturbations in the  $6snl$  Rydberg series. Thus the application of Langer's formula seems preferable to obtain a better fit of the experimental data. However, the former multichannel quantum-defect analyses [18,19] indicate no strong perturbation in the region of large principal quantum numbers studied in the present work, and the valence levels which perturbed the

low-lying Rydberg states seem to have little influence on the  $^1S_0$ ,  $^1P_1$ , and  $^1D_2$  series in the studied region. In fact, a least-squares fit to the general Rydberg-Ritz formula gave satisfactory results with no systematic deviations. In the actual fitting procedure, we calculated the energy difference of

$$\Delta E(n'L'S'J' \leftarrow nLSJ) = \frac{R}{[n - \delta_{LSJ}(n)]^2} - \frac{R}{[n' - \delta_{L'S'J'}(n')]^2} \quad (4)$$

with the approximate expression for the quantum defect,

$$\delta_{LSJ}(n) = \delta_{LSJ0} + \frac{\delta_{LSJ1}}{(n - \delta_{LSJ0})^2} + \dots \quad (5)$$

instead of Eq. (2) for the sake of simplifying the numer-

TABLE I. The  $6sn'p^1P_1 \leftarrow 6sns^1S_0$  transitions.

$n' \leftarrow n$	Observed frequency (MHz)	Calculated frequency (MHz)	Observed minus calculated (MHz)	Measurement linewidth (MHz)
One-photon transition				
$n \leftarrow n$				
35	73407.1	73407.4	-0.3	1.4
36	66682.2	66683.5	-1.3	4.0
37		60755.5		
38		55509.2		
39	50849.4	50849.7	-0.3	1.8
40	46697.9	46697.1	0.8	2.1
41	42984.3	42984.6	-0.3	1.3
42	39655.5	39655.3	0.2	1.9
43 <sup>a</sup>	36660.0	36661.0	-1.0	3.7
44	33961.4	33960.8	0.6	2.9
45	31520.5	31519.4	1.1	2.0
46	29307.1	29306.5	0.6	2.1
47	27296.6	27296.0	0.6	2.8
48	25465.3	25465.3	0.0	4.4
49	23795.5	23794.8	0.7	7.3
50	22267.7	22267.3	0.4	2.6
51	20867.8	20867.8	0.0	1.9
52	19583.6	19583.2	0.4	3.4
53	18401.2	18401.9	-0.7	1.2
$n+1 \leftarrow n$				
52	77077.5	77078.1	-0.6	2.2
53	72485.8	72486.4	-0.6	1.6
54 <sup>a</sup>	68250.0	68252.2	-2.2	4.0
55	64340.7	64341.6	-0.8	2.5
Three-photon transition				
$n \leftarrow n^b$				
34	27022.41	27021.70	0.71	0.41
35	24468.90	24469.15	-0.25	0.42
36	22227.25	22227.83	-0.58	0.40

<sup>a</sup>This transition was excluded from the least-squares fit because of anomalous spectral line shape.

<sup>b</sup>The energy interval and linewidth of this transition corresponds to three times the measured frequency.

TABLE II. The one-photon  $6s(n+2)p^1P_1 \leftarrow 6snd^1D_2$  transitions.

$n$	Observed frequency (MHz)	Calculated frequency (MHz)	Observed minus calculated (MHz)	Measurement linewidth (MHz)
43	74815.67	74815.14	0.53	1.54
44	69537.00	69536.58	0.42	1.61
45	64743.35	64743.31	0.04	2.22
46		60380.81		
47	56402.29	56401.75	0.54	1.38
48	52765.33	52764.91	0.42	1.11
49	49434.38	49434.26	0.12	1.43
50	46378.33	46378.24	0.09	1.43
51	43568.28	43569.12	-0.84	2.00
52	40981.97	40982.45	-0.48	1.39
53	38595.95	38596.63	-0.68	1.74

ical computation. The final fitting parameters are listed in Table VI with the corresponding standard deviations. This fitting was achieved with all the observed frequency data set weighted according to the inverse of measured linewidth except three transitions (see Tables I, III, and IV) which showed anomalous line shapes. These anomalous line shapes originate from experimental artifact because other transitions which share the relevant energy levels in common show normal line shapes. The best fit of the observed frequency data to Eqs. (4) and (5) required the expanded quantum defect terms of up to the third for  $^1S_0$  and  $^1P_1$  series, and to the second for  $^1D_2$  series in Eq. (5). The transition frequencies calculated by Eqs. (4) and (5) with these parameters are also listed in Tables I–V. The calculated quantum defects and term values measured from the ionization limit are given in

the second and third column of Table VII.

Recently Gentile *et al.* [10] reported the microwave spectrum of calcium Rydberg states measured with a similar technique. The  $l$  dependence of  $\delta_0$  and  $\delta_1$  for the two atoms are consistent while the absolute values are much larger for ytterbium. It is interesting to note that the  $\delta_0$ 's of ytterbium have almost the same values as those of barium determined by multichannel quantum-defect theory (MQDT) analysis [29]. However, the  $\delta_1$ 's for ytterbium have opposite sign with much larger absolute values. Since this anomalous behavior of  $\delta_1$  may be due to perturbations, an attempt was made to re-fit our experimental data to the Langer's formula. The perturbers we examined are those used in the former MQDT analysis [18, 19]; two bound states ( $4f^{14}6p^2\ ^1S_0$  at  $48\,762.52\text{ cm}^{-1}$  and  $4f^{13}5d6s6p\ A$  at  $50\,244.38\text{ cm}^{-1}$ ) and

TABLE III. The two-photon  $6s(n+1)s^1S_0 \leftarrow 6sns^1S_0$  transitions. The energy interval and linewidth correspond to twice the measured frequencies.

$n$	Observed frequency (MHz)	Calculated frequency (MHz)	Observed minus calculated (MHz)	Measurement linewidth (MHz)
39	75271.04	75271.30	-0.26	0.67
40	69210.18	69209.81	0.37	0.90
41	63781.70	63781.95	-0.25	0.61
42		58907.05		
43	54516.42	54516.47	-0.05	0.45
44	50551.50	50551.54	-0.04	0.50
45	46962.06	46961.91	0.15	0.61
46	43704.31	43704.21	0.10	0.48
47	40740.96	40740.95	0.01	0.38
48	38039.57	38039.60	-0.03	0.41
49	35571.81	35571.86	-0.05	0.30
50	33312.97	33313.02	-0.05	0.29
51	31241.37	31241.44	-0.07	0.41
52	29337.83	29338.10	-0.27	0.48
53 <sup>a</sup>	27585.10	27586.27	-1.17	0.49
54	25970.78	25971.18	-0.40	0.80
55	24479.52	24479.73	-0.21	0.45
56	23100.14	23100.32	-0.18	0.40

<sup>a</sup>This transition was excluded from the least-squares fit because of anomalous spectral line shape.

TABLE IV. The two-photon  $6s(n+1)d^1D_2 \leftarrow 6sns^1S_0$  transitions. The energy interval and linewidth correspond to twice the measured frequencies.

$n$	Observed frequency (MHz)	Calculated frequency (MHz)	Observed minus calculated (MHz)	Measurement linewidth (MHz)
34	68241.20	68241.24	-0.04	1.33
35		61882.03		
36	56288.60	56288.52	0.08	2.44
37	51348.61	51348.90	-0.29	0.90
38	46970.38	46970.36	0.02	1.37
39	43075.71	43075.48	0.27	0.98
40	39599.91	39599.32	0.59	0.95
41	36487.09	36487.10	-0.01	0.71
42	33692.83	33692.44	0.39	0.93
43 <sup>a</sup>	31177.75	31175.87	1.88	0.81
44	28904.28	28903.66	0.62	1.10
45	26846.92	26846.86	0.06	0.80
46	24980.84	24980.56	0.28	0.52
47	23283.35	23283.21	0.14	0.64
48	21736.13	21736.13	0.00	0.83
49	20322.53	20323.05	-0.52	0.75

<sup>a</sup>This transition was excluded from the least-squares fit because of the anomalous spectral line shape.

two autoionization states ( $50\,988.58$  and  $51\,842.97\text{ cm}^{-1}$ ) for the  $^1S_0$  series, and two bound states ( $4f^{13}5d^26sB$  at  $49\,920.02\text{ cm}^{-1}$  and  $4f^{13}5d^26sC$  around  $50\,380\text{ cm}^{-1}$ ) and the autoionization state expected at  $50\,821\text{ cm}^{-1}$  for the  $^1P_1$  series. However, neither significant improvement of the fit nor identification of the perturber was achieved, indicating the absence of local perturbations in the studied energy region. This is consistent with the result of the Zeeman effect measurement presented in the next section. It will be worthwhile to note that a recent preliminary experiment on the  $D$  states of Rydberg lutetium in our

laboratory revealed still larger values for  $|\delta_1|$ . One possible explanation for the large  $|\delta_1|$  is the large polarization effect in the ion cores of heavy atoms since the negative sign of  $\delta_1$  is consistent with the one observed in the high angular momentum states [30]. Although polarization effects in alkaline-earth atoms is not well studied yet [12, 31] the largest value of  $|\delta_1|$  for  $l=1$  in either atom will be mostly due to the influence of polarization effect which should decrease monotonically with  $l$  ( $l \geq 1$ ). Further studies on high angular momentum states of heavy atoms will be of particular interest in this context.

TABLE V. The two-photon  $6s(n+1)d^1D_2 \leftarrow 6snd^1D_2$  transitions. The energy interval and linewidth correspond to twice the measured frequencies.

$n$	Observed frequency (MHz)	Calculated frequency (MHz)	Observed minus calculated (MHz)	Measurement linewidth (MHz)
38	71795.21	71795.14	0.07	2.59
39	66097.45	66097.59	-0.14	0.40
40		60987.29		
41	56390.46	56390.48	-0.02	0.59
42	52244.45	52244.26	0.19	0.41
43	48494.83	48494.75	0.08	0.61
44	45095.63	45095.61	0.02	0.40
45	42006.90	42006.86	0.04	0.32
46	39193.92	39193.86	0.06	0.27
47	36626.62	36626.53	0.09	0.40
48	34278.59	34278.60	-0.01	0.35
49	32127.16	32127.15	0.01	0.30
50	28335.49	28335.56	-0.07	0.32
52	26662.12	26662.11	0.01	0.32
53	25117.98	25117.88	0.10	0.32
54	23690.72	23690.64	0.08	0.40
55	22369.66	22369.51	0.15	0.40

TABLE VI. Quantum defects determined by fitting the experimental data to Eqs. (4) and (5). Numbers in parentheses are one standard deviations in units of the last significant digits.

Series	Parameters		
	$\delta_0$	$\delta_1$	$\delta_2$
$6sns^1S_0$	4.27914(4)	-7.06(6)	565(25)
$6snp^1P_1$	3.95433(5)	-12.33(6)	1729(27)
$6snd^1D_2$	2.71363(4)	-2.01(4)	

The microwave transitions observed in the present work are all interconnected, forming a network of energy levels among the  $^1S_0$ ,  $^1P_1$ , and  $^1D_2$  Rydberg states (recall that many microwave transitions participate in forming the loops). From these data a set of relative

experimental energies of the Rydberg states were determined by a least-squares fit. Then the whole network of the states were fitted to the calculated energies by adjusting only one parameter, the difference from the ionization energy. The result is given in the fourth column of Table VII. This procedure was taken to find very weak perturbations which were difficult to find only from the transition frequencies. The excellent agreement between the experimental and calculated values implies the absence of weak local perturbations which cause the energy shifts larger than a few MHz as well as correctness of the determined parameters listed in Table VI.

### C. Zeeman effect under a weak magnetic field

Zeeman splittings of the microwave transitions were measured for the  $6snp^1P_1 \leftarrow 6sns^1S_0$  transitions ( $n =$

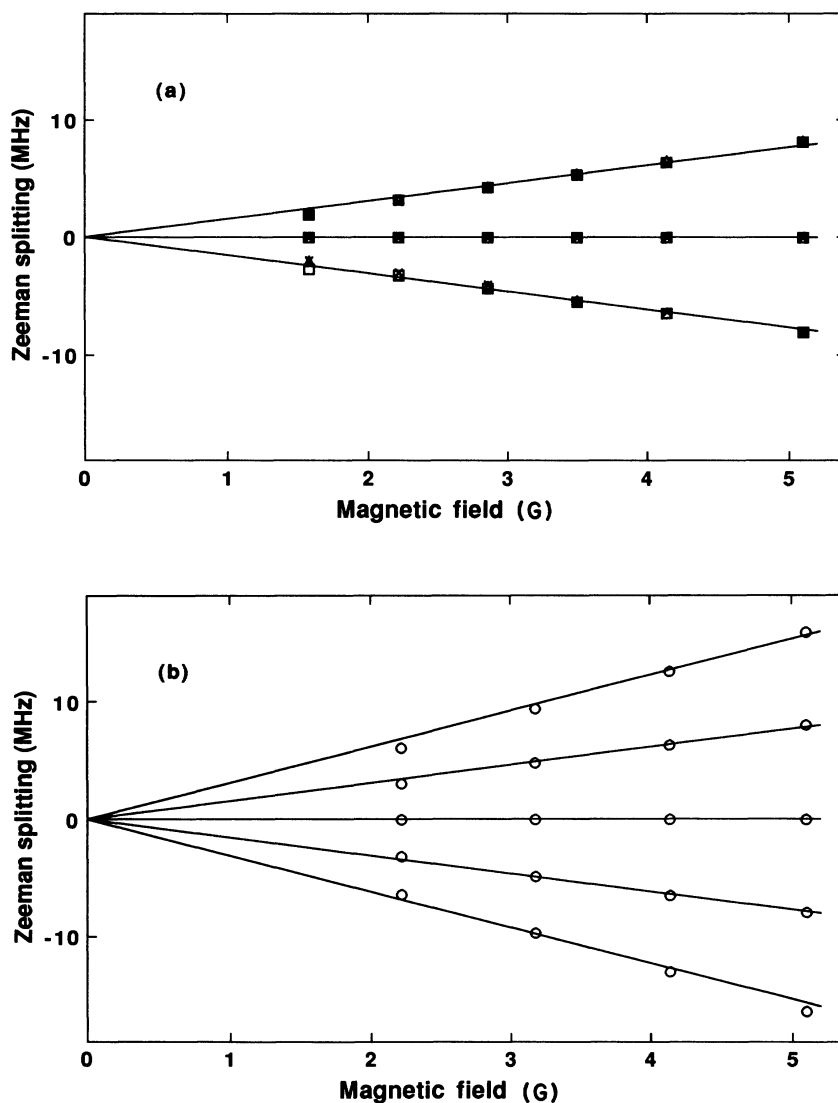


FIG. 6. (a) Zeeman plot of the  $6snp^1P_1 \leftarrow 6sns^1S_0$  transitions for  $n = 35(\Delta)$ ,  $36(\times)$ , and  $47(\square)$ . Solid lines indicate the linear Zeeman shifts for the  $g$  factor of 1.093. (b) Zeeman plot of the  $6snd^1D_2 \leftarrow 6sns^1S_0$  transition for  $n = 37$ . The solid line is the linear Zeeman shift for the  $g$  factor of 1.095.

TABLE VII. Quantum-defect and term values of the  $6sns^1S_0$ ,  $6snp^1P_1$ , and  $6snd^1D_2$  Rydberg states.

$n$	Quantum defect	Energy by Rydberg-Ritz formula (MHz)	Energy by measured data (MHz)	Difference (MHz)
$6sns^1S_0$				
40	4.273955	2577530.26	2577531.23	-0.97
41	4.274216	2439110.63	2439110.82	-0.19
42	4.274458	2311546.74	2311547.42	-0.68
43	4.274683	2193732.63	2193733.01	-0.38
44	4.274893	2084699.68	2084700.17	-0.49
45	4.275088	1983596.59	1983596.83	-0.24
46	4.275271	1889672.77	1889672.79	-0.02
47	4.275442	1802264.35	1802264.18	0.17
48	4.275601	1720782.45	1720782.08	0.37
49	4.275751	1644703.25	1644702.70	0.55
50	4.275892	1573559.52	1573559.22	0.30
51	4.276024	1506933.47	1506933.30	0.17
52	4.276149	1444450.59	1444450.58	0.01
53	4.276266	1385774.39	1385774.65	-0.26
$6snp^1P_1$				
39	3.945438	2677223.09	2677223.90	-0.81
40	3.945865	2530833.03	2530833.33	-0.30
41	3.946264	2396125.99	2396126.52	-0.53
42	3.946637	2271891.41	2271891.92	-0.51
43 <sup>a</sup>	3.946986	2157071.54		
44	3.947313	2050738.82	2050738.77	0.05
45	3.947620	1952077.16	1952076.30	0.86
46	3.947908	1860366.23	1860365.64	0.59
47	3.948179	1774968.29	1774967.72	0.57
48	3.948433	1695317.07	1695316.78	0.29
49	3.948673	1620908.40	1620907.40	1.00
50	3.948898	1551292.19	1551291.63	0.56
51	3.949111	1486065.64	1486065.49	0.15
52	3.949312	1424867.36	1424867.09	0.27
53	3.949502	1367372.41	1367373.27	-0.86
54	3.949681	1313287.97	1313288.77	-0.80
55	3.949851	1262349.57	1262350.46	-0.89
$6snd^1D_2$				
38	2.712016	2641921.85	2641921.88	-0.03
39	2.712104	2498331.58	2498331.46	0.12
40	2.712185	2366136.39	2366136.60	-0.21
41	2.712259	2244161.82	2244161.76	0.06
42	2.712328	2131380.86	2131380.84	0.02
43	2.712391	2026892.34	2026891.94	0.40
44	2.712451	1929902.84	1929902.60	0.24
45	2.712506	1839711.62	1839711.21	0.41
46	2.712557	1755697.90	1755697.54	0.36
47	2.712605	1677310.17	1677309.88	0.29
48	2.712649	1604057.12	1604057.07	0.05
49	2.712691	1535499.91	1535499.87	0.04
50	2.712730	1471245.62	1471245.53	0.09
51	2.712767	1410941.55	1410941.55	0.00
52	2.712802	1354270.43	1354270.65	-0.22
53	2.712834	1300946.21	1300946.41	-0.20
54	2.712865	1250710.45	1250710.45	0.00
55	2.712894	1203329.17	1203329.01	0.16
56	2.712921	1158590.15	1158589.69	0.46

<sup>a</sup>The experimental term value was not calculated since the  $6s43p^1P_1 \rightarrow 6s43s^1S_0$  transition was excluded from the least-squares fit because of its anomalous line shape.

34, 36, and 47) and the  $6s(n-1)d^1D_2 \leftarrow 6sns^1S_0$  transition ( $n = 37$ ). The magnetic field up to  $\sim 5.1$  G was applied to the interaction region with a pair of coils attached to the vacuum chamber. The strength of the magnetic field was calibrated by a G meter with the accuracy of 0.1 G. Since no attempt was made to set the polarization of microwave radiation to a definite direction, the  $\Delta m = 0$  and  $\pm 1$  components were observed simultaneously. In Fig. 6 frequencies of the  $\Delta m = 0$  and  $\pm 1$  Zeeman components relative to the zero-field frequencies are plotted against the magnetic field for the  $6snp^1P_1 \leftarrow 6sns^1S_0$  transition ( $n = 34, 36,$  and  $47$ ) and the  $6s(n-1)d^1D_2 \leftarrow 6sns^1S_0$  transition ( $n = 37$ ). All of the observed  $6snp^1P_1 \leftarrow 6sns^1S_0$  transitions exhibit almost identical first-order Zeeman shifts within the experimental error, and fitting of all these data yields the Landé  $g$  factor, 1.093(43), for the  $^1P_1$  states. However, the triplet mixing parameter calculated from this value gives an embarrassingly large value, approximately 19(9)% which is about three times as large as the values determined by a diamagnetic shift of the  $^1P_1$  Rydberg states [23]. One serious problem in the present measurement is the poor accuracy of magnetic-field measurement while the singlet-triplet mixing parameter is highly sensitive to the measured  $g$  factor. In fact, if the measured magnetic field is 0.2 G lower than the true value, the mixing parameter becomes 6.4% which is the value for  $n = 40$  reported in Ref. [23]. Thus the present measurement does not present the experimental data better

than those in Ref. [23] except that the mixing parameter takes almost the same value for  $n = 34, 36,$  and  $47$ . The  $g$  factor of 1.095(46) for the  $^1D_2$  state determined in the present work is an unacceptable value since the value is beyond the range expected for the mixed  $^1D_2$  state. However, if we use the ratio of these  $g$  factors which will be more reliable because it is the ratio of measured Zeeman shift, and if we assume that the mixing parameter for the  $^1P_1$  states is 6.4% as in Ref. [23], the mixing parameter for the  $6s36d^1D_2$  state is calculated to be 19(6)% where the error arises from 1% uncertainty in the Zeeman shift measurement. This indicates large breakdown of the  $LS$  character for the  $^1D_2$  Rydberg states in comparison with that for  $^1P_1$  Rydberg states. However, this contradicts the experimental results of the MQDT analysis [18] and hyperfine structure measurement [21] that the high Rydberg  $^1D_2$  states have negligibly small triplet mixing. The extended study with improved sensitivity, resolution, and, in particular, with improved accuracy of magnetic-field measurement, is highly desirable for further characterization of the high Rydberg states of ytterbium.

#### ACKNOWLEDGMENTS

We thank Dr. Mizugai for experimental assistance and Professor T. Shimizu for the loan of microwave components. One of us (H.M.) is grateful to Dr. Ahn for useful comments on this work.

- 
- [1] K.B. MacAdam and W.H. Wing, *Phys. Rev. A* **12**, 1464 (1975).
  - [2] T.F. Gallagher, R.M. Hill, and S.A. Edelstein, *Phys. Rev. A* **13**, 1448 (1976).
  - [3] C. Fabre, P. Goy, and S. Haroche, *J. Phys. B* **10**, L183 (1977).
  - [4] C. Fabre, S. Haroche, and P. Goy, *Phys. Rev. A* **18**, 229 (1978).
  - [5] P. Goy, C. Fabre, M. Gross, and S. Haroche, *J. Phys. B* **13**, L83 (1980).
  - [6] C. Fabre, S. Haroche, and P. Goy, *Phys. Rev. A* **22**, 778 (1980).
  - [7] P. Goy, J.M. Raimond, G. Vitrant, and S. Haroche, *Phys. Rev. A* **26**, 2733 (1982).
  - [8] E.A. Hessels, W.G. Sturuss, and S.R. Lundeen, *Phys. Rev. A* **38**, 4574 (1988).
  - [9] E.A. Hessels, F.J. Deck, P.W. Arcuni, and S.R. Lundeen, *Phys. Rev. A* **41**, 3663 (1990).
  - [10] T.R. Gentile, B.J. Hughey, D. Kleppner, and T.W. Ducas, *Phys. Rev. A* **42**, 440 (1990).
  - [11] P. Goy, J. Liang, M. Gross, and S. Haroche, *Phys. Rev. A* **34**, 2889 (1986).
  - [12] T.F. Gallagher, R. Kachru, and N.H. Tran, *Phys. Rev. A* **26**, 2611 (1982).
  - [13] A.G. Vaidyanathan, W.P. Spencer, J.R. Rubbmark, H. Kuiper, C. Fabre, D. Kleppner, and T.W. Ducas, *Phys. Rev. A* **26**, 3346 (1982).
  - [14] T.R. Gentile, B.J. Hughey, D. Kleppner, and T.W. Ducas, *Phys. Rev. A* **40**, 5103 (1989).
  - [15] T.F. Gallagher, W. Sadner, and K.A. Safinya, *Phys. Rev. A* **23**, 2969 (1981).
  - [16] J.F. Wyart and P. Camus, *Phys. Scr.* **20**, 43 (1979).
  - [17] P. Camus, A. Débarre, and C. Morillon, *J. Phys. B* **13**, 1073 (1980).
  - [18] M. Aymar, A. Débarre, and O. Robaux, *J. Phys. B* **13**, 1089 (1980).
  - [19] M. Aymar, R.J. Champeau, C. Delsart, and O. Robaux, *J. Phys. B* **17**, 3645 (1984).
  - [20] B.R. Wu, Y.F. Zheng, Y.F. Xu, L.G. Pan, J. Lu, and J.W. Zhong, *J. Phys. B* **24**, 49 (1991).
  - [21] L. Barbier and R.J. Champeau, *J. Phys. (Paris)* **41**, 947 (1980).
  - [22] U. Majewski, J. Neukammer, and H. Rinneberg, *Phys. Rev. Lett.* **51**, 1340 (1983).
  - [23] J. Neukammer, H. Rinneberg, and U. Majewski, *Phys. Rev. A* **30**, 1142 (1984).
  - [24] T.W. Ducas, M.G. Littman, R.R. Freeman, and D. Kleppner, *Phys. Rev. Lett.* **35**, 366 (1975).
  - [25] D.R. Hartree, *Proc. Camb. Philos. Soc.* **24**, 426 (1928).
  - [26] R.M. Langer, *Phys. Rev.* **35**, 649 (1930).
  - [27] A.G. Shenstone and H.N. Russell, *Phys. Rev.* **39**, 415 (1932).
  - [28] W.R.S. Garton, *J. Quant. Spectrosc. Radiat. Transfer* **2**, 335 (1962).
  - [29] J.J. Wynne and J.A. Armstrong, *IBM J. Res. Dev.* **23**, 490 (1979).
  - [30] See, for example, B. Edlén, in *Encyclopedia of Physics* (Springer, Berlin, 1964), Vol. XXVII, p. 123.
  - [31] J.H. Van Vleck and N.G. Whitelaw, *Phys. Rev.* **44**, 551 (1933).